FERROELECTRIC TUNGSTEN BRONZE BULK CRYSTALS AND EPITAXIAL THIN FILMS FOR ELECTRO-OPTIC DEVICE APPLICATIONS

Semi-Annual Technical Report No. 5
For Period 10/01/84 through 03/31/85

JULY 1985

The views and conclusions contained in this document are those of the authors and should not be interpreted as necessarily representing the official policies, either expressed or implied, of the Defense Advanced Research Projects Agency or the United States Government.

85 09 17 184

AD-A159 279

REPORT DOCUMENTATION PAGE

1a. REPORT SECURITY CLASSIFICATION	1b. RESTRICTIVE MARKINGS
Unclassified	

2a. SECURITY CLASSIFICATION AUTHORITY	3. DISTRIBUTION/AVAILABILITY OF REPORT
2b. DECLASSIFICATION/DOWNGRADING SCHEDULE	Approved for public release; distribution unlimited.

4. PERFORMING ORGANIZATION REPORT NUMBER(S)	5. MONITORING ORGANIZATION REPORT NUMBER(S)
SC5340.10SA	P2D10

6a. NAME OF PERFORMING ORGANIZATION	6b. OFFICE SYMBOL (If applicable)	7a. NAME OF MONITORING ORGANIZATION
Rockwell International Science Center		Defense Advanced Research Projects Agency (DoD)

6c. ADDRESS (City, State and ZIP Code)	7b. ADDRESS (City, State and ZIP Code)
1049 Camino Dos Rios Thousand Oaks, CA 91360	1400 Wilson Boulevard Arlington, VA 22209

8a. NAME OF FUNDING/SPONSORING ORGANIZATION	8b. OFFICE SYMBOL (If applicable)	9. PROCUREMENT INSTRUMENT IDENTIFICATION NUMBER
Naval Research Laboratory		Contract No. N00014-82-C-2466

8c. ADDRESS (City, State and ZIP Code)	10. SOURCE OF FUNDING NOS			
4555 Overlook Avenue S.W. Washington, DC 20375	PROGRAM ELEMENT NO.	PROJECT NO. DARPA ORDER NO. 4540	TASK NO.	WORK UNIT NO.

11. TITLE (Include Security Classification) GROWTH OF FERRO-ELECTRIC TUNGSTEN BRONZE EPITAXIAL THIN FILMS FOR ELECTRO-OPTIC DEVICE APPLICATIONS

12. PERSONAL AUTHOR(S)
Olivar, John R.

13a. TYPE OF REPORT	13b. TIME COVERED	14. DATE OF REPORT (Yr., Mo., Day)	15. PAGE COUNT
Semi-Annual Technical No. 5	FROM 10/01/84 TO 03/31/85	AUGUST 1985	46

16. SUPPLEMENTARY NOTATION
The views and conclusions contained in this document are those of the authors and should not be interpreted as necessarily representing the official policies, either expressed or implied, of the Defense Advanced Research Projects Agency or the United States Government.

17	COSATI CODES		18. SUBJECT TERMS (Continue on reverse if necessary and identify by block number)
FIELD	GROUP	SUB GR.	SBN, Ce and Fe Doping, Photorefractive Materials, Focal Plane Array, Czochralski Growth, Striations, Thermodynamic Phenomanology, Thermodynamic Constants, Tungsten Bronze Ferroelectrics

19. ABSTRACT (Continue on reverse if necessary and identify by block number)

Several doped (Ce^{3+}/Ce^{4+} and Fe^{2+}/Fe^{3+}) and undoped SBN:60 single crystals have been grown using the Czochralski technique. Optical evaluation shows that Ce-doped crystals have minimum or no striations and are of optical quality, while Fe-doped crystals are highly striated under all growth conditions. Current results suggest that the existence of striations depends strongly on the type of dopant and its location in the structure. Ce-doped SBN:60 crystals currently exhibit excellent photorefractive properties with improved sensitivity and speed, indicating possible use for this material in device applications.

The bronze composition SBN:50 is being studied for pyroelectric IR focal plane array applications. SBN:50 is slightly off congruent melting; however, using the current Czochralski technique it is now possible to grow good quality crystals as large as 1 cm in diameter.

An extensive discussion of the thermodynamic phenomenology for tungsten bronze crystals is presented. An excellent fit to birefringence polarization data for $Ba_2NaNb_5O_{15}$ (BNN) is found for the Devonshire form of the Gibbs free-energy expansion, and good agreement is found for a number of thermodynamic constants over a

20. DISTRIBUTION/AVAILABILITY OF ABSTRACT	21. ABSTRACT SECURITY CLASSIFICATION
UNCLASSIFIED/UNLIMITED ☒ SAME AS RPT. ☐ DTIC USERS ☐	Unclassified

22a. NAME OF RESPONSIBLE INDIVIDUAL	22b. TELEPHONE NUMBER (Include Area Code)	22c. OFFICE SYMBOL

DD FORM 1473, 83 APR   EDITION OF 1 JAN 73 IS OBSOLETE.

(Block 19 Continued)

broad range of tungsten bronze materials. This indicates that the hypothesis of near-constant higher order stiffness parameters is a good approximation for tetragonal bronze ferroelectrics, thereby allowing the analysis of a very wide range of other bronze compositions.

Rockwell International
Science Center

SC5340.10SA

TABLE OF CONTENTS

LIST OF FIGURES

LIST OF TABLES

1.0 SUMMARY AND PROGRESS

Tungsten bronze (T.B.) family crystals have been shown to be useful for a number of device applications, including electro-optic waveguides, photore-fractive holography and pyroelectric FPA. The current work reports on the development of good quality (acceptable for device studies) $Sr_{1-x}Ba_xNb_2O_6$, $x = 0.40$ and 0.50, and morphotropic phase boundary compositions. The composition SBN:60 has been used for electro-optic and nonlinear optical applications, while SBN:50 will be developed for pyroelectric FPA applications. Considerable progress has been made in several areas, including the growth of Ce- and Fe-doped SBN:60 crystals. Based on current work, a number of new dopants have also been identified for both photorefractive and pyroelectric studies. This work also includes the continued effort to search for new T.B. systems specifically based on morphotropic phase boundary compositions for photorefractive and transverse pyroelectric FPA applications.

Several doped (Ce^{3+}/Ce^{4+} and Fe^{2+}/Fe^{3+}) and undoped SBN:60 single crystals have been grown using the Czochralski technique. Optical evaluation shows that Ce-doped crystals have minimum or no striations and are of optical quality, while Fe-doped crystals are highly striated under all growth condi-tions, and the striations are found difficult to suppress. In the tungsten bronze structure, Ce^{3+} and Ce^{4+} are expected to occupy the 12- and 9-fold co-ordinated sites, while Fe^{2+} and Fe^{3+} ions are expected to occupy 6-fold coordi-nated sites. Our current results suggest that the existence of striations in SBN:60 crystals depends strongly on the type of dopant and its location in the structure. Since Mn^{2+}, Co^{2+} and Cr^{3+}, etc., have ionic size and site prefer-ences similar to Fe^{3+}, it will be interesting to check their influence on striations in SBN:60 crystals. Ce-doped SBN:60 crystals currently exhibit excellent photorefractive properties with improved sensitivity and speed, indicating possible use for this material in device applications.

Since the composition SBN:50 has a higher Curie temperature (110 - 120°C) and also an excellent figure-of-merit for pyroelectric FPA applications,

a systematic study of this crystal has recently been initiated. This composition is slightly off congruent melting; however, using the current Czochralski technique it has been possible to grow good quality crytals as large as 1 cm in diameter. Efforts are now underway to establish its pyroelectric and dielectric properties for FPA applications.

An extensive discussion of the thermodynamic phenomenology for tungsten bronze crystals is presented in the Appendix along with a tabulation of a number of thermodynamic constants based on current research and other data in the literature. An excellent fit to birefringence polarization data for $Ba_2NaNb_5O_{15}$ (BNN) is found for the Devonshire form of the Gibbs free-energy expansion, and good agreement is found for a number of thermodynamic constants over a broad range of tungsten bronze materials. This indicates that the hypothesis of near-constant higher order stiffness parameters is a good approximation for tetragonal bronze ferroelectrics, thereby allowing the analysis of a very wide range of other bronze compositions.

2.0 DEVELOPMENT OF OPTICAL QUALITY SBN CRYSTALS

2.1 Material Growth Techniques

Most of the bronze compositions grown in our laboratory are based on solid solution systems; therefore suitable growth techniques to produce crystals free of optical defects such as striations, scattering centers and twinning must be developed. Striations and other defects are typical problems common to solid solution crystals, and it is often difficult to suppress them completely. However, these problems can be reduced effectively such that the crystals can be useful for optical device studies. The difficulty of this task underscores the criticality of selecting appropriate growth techniques in the present work. At present, three different techniques have been chosen to develop SBN and other bronze crystals. They are as follows:

1. Bulk Single Crystals: Czochralski technique

2. Thin Films: Liquid phase epitaxy (LPE)

3. Strip Crystals: Edge defined film-fed technique

The first two techniques are well established in our current work, and bulk crystals and films of SBN compositions have already been grown. In the present report, the continued growth of striation-free SBN crystals is discussed along with associated growth problems.

2.2 Growth Procedure

Nb_2O_5, $SrCO_3$, Fe_2O_3, CeO_2 and $BaCO_3$ fine powders have been used as starting materials and have been weighed out in the desired proportions, as summarized in Table 1. The batch mixture is ball-milled in acetone for 20-30 h, and then is poured into a large drying dish. The dried powder is placed in a platinum reactic dish and is calcined at 1000°C for 10-15 h to eliminate carbonates and any possible carbon from the pyrolytic breakdown of residual acetone. The calcined powder is then ball-milled and refired in an oxygen flow of 2 cfh at 1400°C for about 4 - 6 h. Phase checks and x-ray lattice constant

Table 1

Materials for Bulk Single Crystal SBN:60 Growth

Crystal Composition	Starting Materials		Conditions and Remarks
SBN:60	a. $SrCO_3$	135.08 gms	Congruent melting composition
	b. $BaCO_3$	115.48 gms	Large crystals can be grown
	c. Nb_2O_5	398.73 gms	Large electro-optic coefficient (r_{33})
	Total wt.	649.26 gms	Melts at 1510°C
	Growth wt.	450.00 gms	Crack-free and optical quality
SBN:60 + Fe^{3+}	a. $SrCO_3$	135.08 gms	Dielectric and electro-optic
	b. $BaCO_3$	115.48 gms	coefficient increased
	c. Nb_2O_5	398.73 gms	Growth of large crystals is
	d. Fe_2O_3	1.98 gms	possible
		to	Enhanced photorefractive
		3.05 gms	properties
	Total wt.	651.24 gms	Crack-free crystals
	Growth wt.	450.00 gms	
SBN:60 + Ce^{3+}	a. $SrCO_3$	135.08 gms	Dielectric and electro-optic
	b. $BaCO_3$	115.48 gms	coefficient improved
	c. Nb_2O_5	398.73 gms	Growth of large crystals is
	d. CeO_2	1.00 gms	possible
		to	Enhanced photorefractive
		1.50 gms	properties
	Total wt.	650.26 gms	Crack-free and optical quality
	Growth wt.	450.00 gms	crystals

measurements are made for each batch to ensure the use of a phase-pure bronze composition for crystal growth. A thick-walled platinum crucible of 2 × 2 in. in dimension is used for this growth, and this container holds roughly 450 g of melt composition.

2.3   Growth of $Sr_{1-x}Ba_xNb_2O_6$, x = 0.40 and 0.50

As summarized in Table 2, we have grown a number of doped and undoped SBN:60 and SBN:50 single crystals of excellent quality using the Czochralski technique. Small amounts of impurities have been shown to have a drastic photorefractive effect in optical applications. According to the current device need, the growth compositions have been modified as follows:

    a.   Optical Waveguide (NRL):   High optical quality starting materials to avoid photorefrctive and striation effects. SBN:60 composition has only been used for this task.

    b.   Photorefractive Studies: High optical quality starting materials with specific impurities, e.g., Ce or Fe, in SBN:60.

    c.   Pyroelectric Studies: High optical quality starting materials. Main emphasis on the SBN:50 composition.

2.4   Growth of Doped SBN:60 Crystals

The main objective of this task is to enhance the photorefractive sensitivity and speed of ferroelectric SBN:60 single crystals using specific impurity species. The current trend in ferroelectric materials indicates that the photorefractive sensitivity of SBN:60 is very large, on the order of 10^{-3} or higher. However, the response time for these crystals is relatively slow when compared with the best known nonferroelectric cubic $Bi_{12}SiO_{20}$ (BSO) crystals, which have a response time typically on the order of 1 ms.

To improve response time and sensitivity, considerable progress has been made using appropriate dopants in materials such as SBN:60, $KNbO_3$, $BaTiO_3$, and $LiNbO_3$. The most commonly used dopants in these crystals include Fe^{2+}/Fe^{3+}, Ce^{3+}/Ce^{4+}, Mo^{4+}/Mo^{6+}, and U^{4+}/U^{6+}. To develop high sensitivity and fast response in tungsten bronze SBN:60 crystals, effort has focussed on the

Table 2
Growth of SBN:60 and SBN:50 Crystals

Boule No. 2	Date Grown	Boule wt.	Dip °C	Rotation rpm	Remarks, Observations
185	05/29/84	16.7	1491	5-8	Uncracked
186	06/01/84	34.6	1489	~ 8	Neck nearly defect-free
187	06/06/84	38.3	1491	~ 8	ADC used, uncracked
188	06/12/84	25	1482	5-15	New charge - flat top, heavily defected, cracks 5 nines purity - less color
189*	06/18/84	25.3	1484	~10	Uncracked - appears core-free
190	06/21/84	18.6	1485	10-12	Uncracked - core-free
191	07/10/84	27.8	1485	8-10	Uncracked - had to de-twin
192	07/13/84	14.3	1486	10	One deep twin - cracked along one side
193	07/30/84	27	1480	~12	Minor coring, uncracked
194	08/02/84	38	1485	10	Good ADC, uncracked core-free boule
195*	08/23/84	42.5	1485	~10	1.8-1.9 cm dia, uncracked
196	08/27/84	49	1485	10	2.0 cm dia, uncracked
197	08/30/84	29	1490	10	Uncracked
198	09/11/84	~5	1490	10	Test new load cell (test crystal)
199	09/25/84	29.5	1485	12	Test new crucible support (small boule)
200	09/28/84	52.5	1485	5-10	Small bubble in boule neck ~19 mm dia
201	10/03/84	41	~1485	5-10	Pink color boule, 19 mm di
202	10/05/84	41	~1485	5-10	Pink color, 18 mm dia Minor twinning
203	10/10/84	18	~1485	~10	Pink, uncracked
204	10/18/84	35.7	~1485	5-10	Dark pink, no twins, uncracked
205	10/30/84	~15	~1485	10-15	Wine color, uncracked

*To NRL

Rockwell International
Science Center

increase of the space charge field, E, since the change in refractive index, Δn, is linearly proportional to E from the relation

$$\Delta n = 1/2 \, n_1^3 r_{ij} E_j \quad , \tag{2.1}$$

where r is the electro-optic coefficient.

Table 3 summarizes the various dopants selected in the present study, their valence states, and their anticipated site preferences in the tungsten bronze structure. Since the role of Fe^{2+}/Fe^{3+} and Ce^{3+}/Ce^{4+} has been widely studied in various ferroelectric crystals, the present work has concentrated on these dopants. The growth and feasibility of SBN:60 crystals doped with these ions have been discussed in our previous report. Since then, considerable progress has been made to improve the quality of these crystals for potential use in photorefractive device applications.

Table 3
Role of Dopants in SBN:60

Dopant	Site Preference				Configuration	Basis	°C	Dielectric Constant	Comments
	15-fold	12-fold	9-fold	6-fold					
Ce^{3+}	-	Ce^{3+}	-	-	$4f^1 5s^2 p^6$	$^2F_{5/2}$	Reduced	Increased	Large Crystals
Ce^{4+}	-	Ce^{4+}	Ce^{4+}	Ce^{4+}	-	-	Reduced	Increased	Large Crystals
Fe^{3+}	-	-	-	Fe^{4+}	$3d^5$	$^6S_{5/2}$	Reduced	Increased	Large Crystals
Fe^{2+}	-	-	Fe^{2+}	Fe^{2+}	$3d^6$	$^5D_4$	-	Increased	Large Crystals
Cr^{3+}	-	-	-	Cr^{3+}	$3d^3$	$^4F_{3/2}$	-	-	-
Mn^{2+}	-	-	Mn^{2+}	Mn^{2+}	$3d^5$	$^6S_{5/2}$	-	-	-
Mn^{3+}	-	-	-	Mn^{3+}	$3d^4$	$^5D_0$			
Nb^{4+*}							Reduced	Increased	Large Crystals

*Nb^{5+} reduces to Nb^{4+} at high temperature.

Recently, we successfully demonstrated the growth of Ce- and Fe-doped SBN:60 single crystals as part of our effort to study in detail the role of these ions in photorefractive device applications. As shown in Fig. 1 approximately 1 to 2 cm diameter Ce- and Fe-doped SBN:60 crystals have been grown along the (001) direction using the Czochralski technique. Doping of SBN:60 with Fe, and Fe and Ce together, has not been done previously, and Fe is expected to produce interesting results, as it has been observed to do in other ferroelectric crystals such as $LiNbO_3$ and $KNBO_3$.

Ce-doped SBN:60 crystals show minimum or no striations, and the crystals are of optical quality, while Fe-doped crystals are highly striated under all growth conditions, and the striations are found difficult to suppress. In the tungsten bronze structure, Ce^{3+} and Ce^{4+} are expected to occupy the 12- and 9-fold coordinated sites, while Fe^{2+} and Fe^{3+} ions are expected to occupy 6-fold coordinated sites. Our results suggest that the existence of striations in SBN:60 crystals depends strongly on the type of dopant and its location in the structure. Since Mn^{2+}/Mn^{3+}, Co^{2+}/Co^{3+}, Ti^{3+}/Ti^{4+}, etc., have ionic size and site preference similar to Fe^{3+}, it will be interesting to check their influence on striations in SBN:60 crystals.

The development of striation-free Ce-doped SBN:60 crystals makes possible the evaluation of the photorefractive properties, specifically sensitivity and speed. Typical $6 \times 6 \times 6$ mm size cubes have been supplied for examination, and two- and four-wave mixing techniques are being used. These measurements are being made at Caltech and other laboratories, and will be reinvestigated as better quality crystals become available. Table 4 summarizes the proposed goals set and results obtained to date for SBN:60 crystals. In agreement with the results reported by Megumi et al,[1] the present crystals show the typical Ce broad absorption band around 0.50 μm, and this band remains unchanged from one sample to another.

SC85-32578

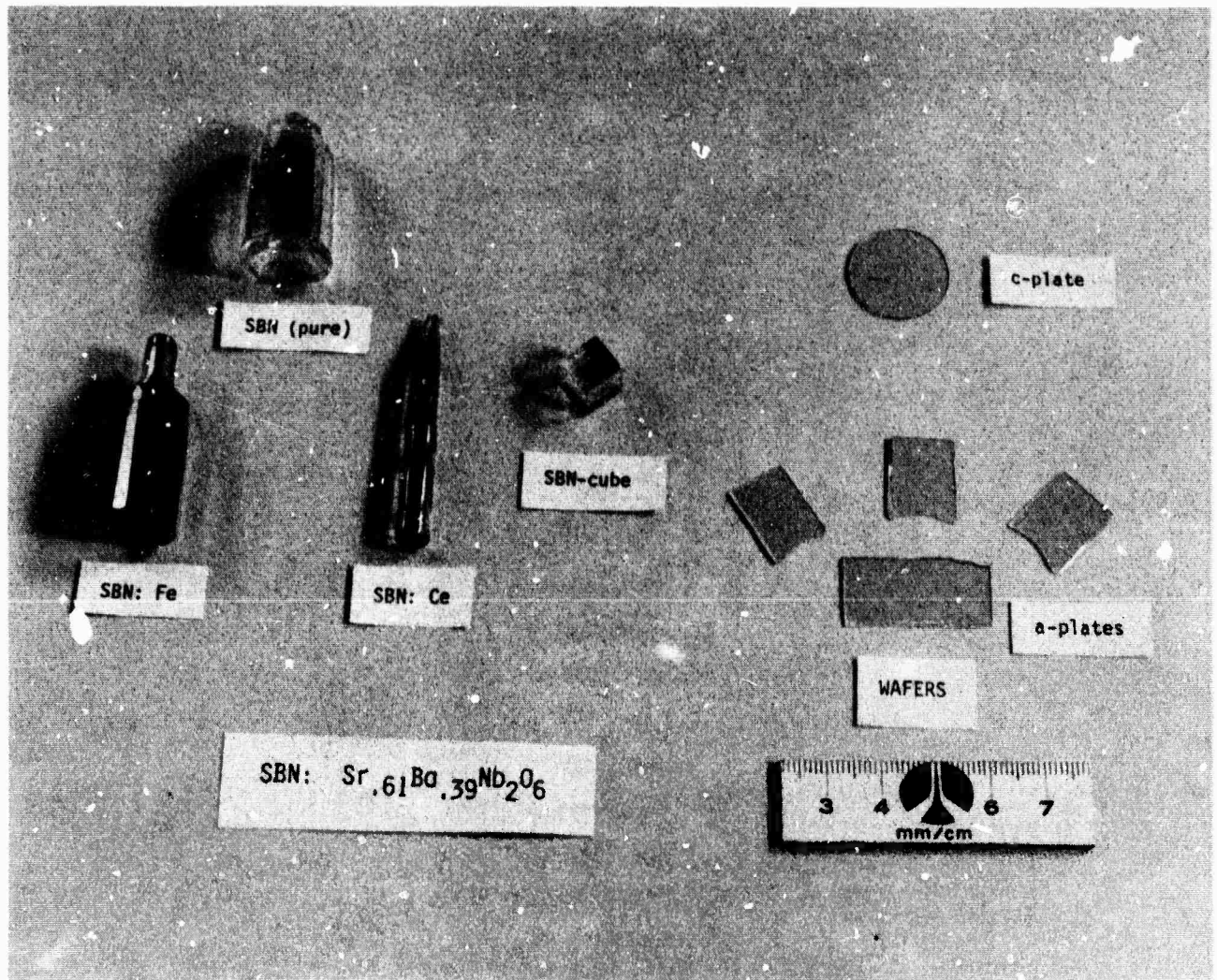Fig. 1 Doped and undoped SBN:61 single crystals grown
at the Rockwell International Science Center.

Table 4

Goals for Photorefractive Studies and Current Results

Desired Properties	Observed Properties
1. Response time ~ 1 ms	1. Response time achieved < 100 ms
2. Sensitivity $\sim 10^{-4}$ to 10^{-5} cm^2/J	2. Sensitivity achieved $\sim 10^{-3}$ cm^2/J
3. Coupling coefficient ~ 1 cm^{-2}	3. Coupling coefficient achieved ~ 11 cm^{-1}
4. Large size, optical quality crystals	4. Large size (2.5 cm in diameter) and striation-free SBN:60 and Ce^{3+}-doped SBN:60 crystals are available
5. Large electro-optic coefficient necessary	5. Electro-optic coefficient enhanced for Fe^{3+} and Ce^{3+} additions

A useful evaluation method for the photorefractive sensitivity of electro-optic crystals is the sensitivity, S, defined as the index change per absorbed energy density,

$$S = \frac{\Delta n}{\Delta W_{abs}} \tag{2.2}$$

For 0.1 wt% Ce-doped crystals, this sensitivity was measured to be 6.5×10^{-3} cm^2/J. This value is in close agreement with the value reported by Megumi et al.,[1] and exceeds that of Fe-doped $LiNbO_3$ and $Mo^{4\pm}$ and $Fe^{3\pm}$ doped $Ba_2NaNb_5O_{15}$ by more than two orders of magnitude. For this addition, the response time also changed, becoming faster (~ 80 to 100 msec) compared to undoped crystals (~ 00 msec). These are considered to be significant improvements, and although details regarding the photorefractive mechanisms are not yet known with certainty, it appears that one can improve both the response time and sensitivity with suitable dopants. Fe-doped crystals also show similar improvements; however, the estimation of precise values has been difficult due to marginal crystal quality. Efforts are now underway to investigate the striation problems associated with Fe-doped SBN:60 crystals.

The improvement in photorefractive characteristics needs to be related to the possible roles of these impurities. In the ideal picture, one needs both

a donor of electrons and an acceptor to enhance the space charge field E_1.
These might be Ce^{3+} and Ce^{4+}, Fe^{2+} and Fe^{3+}, Ce^{3+} and Fe^{3+}, or combinations of
these with Nb^{4+} and various vacancies in the SBN:60 structure. The current
results clearly indicate that the addition of Ce and Fe dopants enhances the
photorefractive properties; however, the ratio of the various charge states of
Ce^{3+}/Ce^{4-} or Fe^{2+}/Fe^{3+} has not yet been established. Because Ce^{3+} (or Fe^{3+}) is
stable at the growth temperature, there exist several possibilities for the
species which form charge traps, as shown in Table 5. In the present case, the
tendency of Nb^{5+} to reduce to Nb^{4+} provides the possibility of donor states.
Since the preferred state of Ce at the growth temperature is Ce^{3+}, a donor,
there is some question concerning the identity of the acceptor level in Ce-doped
crystals. The observed tendency of Nb^{5+} to reduce at the growth temperature may
encourage the formation of vacancies, which would act as either donors or accep-
tors. Currently, we are using optical and Mössbauer spectroscopy to identify
the donor and acceptor species in these crystals. Once this is accomplished, it
should be possible to control both the sensitivity and speed in a more effective
manner.

Table 5
Valance States of Dopants in SBN

Dopant	Crystallographic Sites				Donor	Acceptor	Stable States*
	15-	12-	9-	6-			
Ce^+	-	Ce^{3+}	Ce^{4+}	--	Ce^{3+}	Ce^{4+}	Ce^{3+}
Ce and Nb	-	Ce^{3+}	Ce^{4+}	Nb^{4+}	Ce^{3+}, Nb^{4+}	Ce^{4+}	Ce^{3+}, Nb^{5+}
Ce	-	Ce^{3+}	--	--	Ce^{3+}	Cation Vac.	Ce^{3+}
Fe	-	--	--	Fe^{2+}, Fe^{3+}	Fe^{2+}	Fe^{3+}	Fe^{3+}
Fe, Nb	-	--	--	Fe^{3+}, Nb^{4+}	Nb^{4+}	Fe^{3+}	Fe^{3+}, Nb^{5+}
Fe	-	--	--	Fe^{3+}	Cation Vac.	Fe^{3+}	Fe^{3+}
Ce, Fe	-	Ce^{3+}	--	Fe^{3+}	Ce^{3+}	Fe^{3+}	Ce^{3+}

*Valance state at growth temperature,
Vac. - Vacancy

The improvement in photorefractive properties obtained by doping SBN:60 crystals presents a unique opportunity to study new device concepts. At the same time, these studies are providing the basis for understanding the photorefractive mechanism responsible for these improvements, as well as guiding the search for new classes of electro-optic materials. For the next six months the following aspects of SBN crystal growth will be studied:

- Establish the valence states of Ce in SBN:60 single crystals.

- Establish whether any free Nb^{4+} is present in SBN:60 crystals and its effect on photorefractive properties.

- Improve the current growth technique to suppress the striations present in Fe-doped SBN:60 crystals. Also, establish the concentration at which striations appear.

- Identify another suitable dopant which will occupy the 6- or 9-fold coordinated sites, e.g., Cr^{3+}/Fe^{3+}, Co^{2+}/Co^{3+}, Ti^{3+}/Ti^{4+}, or other cations.

- Establish the ferroelectric and electro-optic properties with respect to new dopants and evaluate their potential suitability in photorefractive applications.

2.5   SBN:50 Crystals for Pyroelectric Studies

The development of doped or undoped $Sr_{1-x}Ba_xNb_2O_6$, x = 0.50, single crystals for pyroelectric focal plane array (FPA) applications is a new task under this contract for the 1985-1987 period. Although contract funding was not available at the time when this work was initiated, we began to study the factors that influence the figure-of-merit for this application. At the present time, the figure-of-merit for a FPA is defined as $p/\sqrt{\epsilon}$, where p is the pyroelectric coefficient and ϵ is the dielectric constant, and this value is significantly higher for SBN:50 crystals as compared to many other ferroelectric crystals, as listed in Table 6.

Table 6
Leading Pyroelectric Materials

Crystal Composition	T_c (°C)	Dielectric Constant at 23°C	Pyroelectric Coefficient × 10^{-10} c/cm^{-2} K^{-1}	Figure-of-Merit	
				P/ϵ	$P/\sqrt{\epsilon}$
TGS	49	28	310	11.07	58.58
TGS:P^{5+}*	50	-	-	-	-
LiTaO$_3$	660	49	170	3.47	24.28
SBN:60	75	500	850	1.82	38.01
SBN:50	128	300	680	2.28	39.26
SBN:50, 0.5% La^{3+}	106	485	1562	3.22	70.92
BSKNN	208	120	485	4.04	44.27
Pb$_5$Ge$_3$O$_{11}$	152	36	110	3.065	18.33

*Work is in progress to obtain optimum dopant concentration.

Based on the currently accepted figure-of-merit, clearly for the longitudinal FPA applications, it is important to maintain a high pyroelectric coefficient and a sufficiently low dielectric constant. In the case of SBN:50, the dielectic constant is relatively low; however, a crystal chemical approach is being used to study suitable dopants that will maintain a high pyroelectric coefficient and further reduce the dielectric constant. We have examined the role of various ions in SBN:50 using ceramic samples, and have found that non-3d or 4f ions (e.g., La^{3+}) are suitable to enhance the pyroelectric figure-of-merit, while other ions are unsuitable since they increase the dielectric losses. Table 7 summarizes the results of addition of various ions in different crystallographic sites and their influence on the pyroelectric figure-of-merit.

Table 7
Effect of Dopants in SBN Crystals

| Dopant | Crystallographic Site | | | | P | ϵ | Tan δ |
	15-Fold	12-Fold	9-Fold	6-Fold			
La^{3+}	La^{3+}	La^{3+}	--	--	Increased	Increased	--
Ca^{2+}	--	Ca^{2+}	--	--	Increased	Increased	Reduced
Eu^{3+}, Sm^{3+}	Eu^{2+}, Sm^{2+}	Eu^{3+}, Sm^{3+}	--	--	Increased	Increased	Increased
K^+, Ti^{4+}	K^+	K^+	--	Ti^{4+}	--	Reduced	Reduced
Fe^{3+}, Ce^{3+}	--	Ce^{3+}	--	$Fe^{2+/3+}$	Increased	Increased	Increased

Since the addition of La^{3+} and Ca^{2+} favors the enhancement of the pyroelectric figure-of-merit, the growth of La^{3+}-doped SBN:50 compositions has been initiated. The substitution of La^{3+} in SBN:50 has been studied earlier by Liu et al.,[2] and they were successful in growing small crystals, typically 0.5 to 1.0 cm in diameter. At Rockwell we have been successful in developing excellent quality La^{3+}-doped SBN:50 crystals up to 1.7 cm in diameter. This is a significant achievement, and we plan to develop still larger crystals for pyroelectric studies. We will continue to develop the growth technique for this composition during the next six months, and we plan also to evaluate its properties with respect to FPA device requirements.

3.0 THE PHOTOREFRACTIVE EFFECT IN UNDOPED
AND DOPED SBN:60

The photorefractive effect in strontium barium niobate (SBN) has now been studied both experimentally and theoretically at Caltech. In particular, we have demonstrated that the introduction of cerium into SBN has resulted in a crystal with a significantly greater photorefractive response.[3] To explain these results, the band transport model for SBN was presented.[4] This theoretical model addressed two-wave mixing in SBN on a microscopic level. This phenomenon is frequently used in the characterization of photorefractive materials[5] and is, therefore, described below.

Consider the two-wave mixing experiment shown in Fig. 2. Beams 1 and 2 are plane waves which intersect in the crystal and thus form an intensity interference pattern. Charge is excited by this periodic intensity distribution into the conduction band, where it migrates under the influence of diffusion and drift in the internal electric field, and then preferentially recombines with traps in regions of low irradiance. A periodic space charge which modulates the refractive index via the electro-optic effect is thus created. This index grating, being out of phase with the intensity distribution, introduces an asymmetry that allows one beam to be amplified by constructive interference with light scattered by the grating, while the other beam is attenuated by destructive interference with diffracted light. This process is shown graphically in Fig. 3.

Mathematically, this two-beam coupling may be described in the steady-state as follows:

$$\frac{dI_1}{d\xi} = -\Gamma\frac{I_1 I_2}{I_1 + I_2} - \alpha I_1 \tag{3.1}$$

$$\frac{dI_2}{d\xi} = \Gamma\frac{I_1 I_2}{I_1 + I_2} - \alpha I_2 \tag{3.2}$$

where I_1, I_2 are the intensities of beams 1 and 2 <u>inside</u> the crystal respectively, Γ is the two-beam coupling coefficient, α is the absorption coefficient and $\xi \equiv z/\cos\theta_1$ where $o < \xi < \ell \equiv d/\cos\theta_1$. The transient behavior is modeled by the following:

$$I_i(\xi;t) = (1-e^{-t/\tau})I_i(\xi;t\to\infty) + e^{-t/\tau}I_i(\xi;t=0), \quad i=1,2 \qquad (3.3)$$

where τ is a characteristic time constant and

$$I_i(\xi;t\to\infty) \equiv I_i(\xi).$$

The solutions of the above coupled wave equations are

$$I_1(\ell) = \frac{[I_1(0) + I_2(0)]e^{-\alpha\ell}}{1 + \dfrac{I_2(0)}{I_1(0)} e^{\Gamma\ell}} \qquad (3.4)$$

$$I_2(\ell) = \frac{[I_1(0) + I_2(0)]e^{-\alpha\ell}}{1 + \dfrac{I_1(0)}{I_2(0)} e^{-\Gamma\ell}} \qquad (3.5)$$

By measuring the four intensities I_1 (0), I_2 (ℓ), and I_2 (ℓ), both in the steady-state and as a function of time, the two-beam coupling coefficient Γ and the response time τ can, therefore, be obtained from the above equations.

However, both Γ and τ can be derived from first principles using the band transport model.[4] Solutions to the photorefractive equations developed most fully by Kuhtarev[6-8] show that Γ and τ can be represented functionally as follows:

$$\Gamma = \Gamma(k_g, E_o, \lambda, T; r, N_D, N_A, \epsilon, n)$$

$$\tau = \tau(k_g, E_o, \lambda, T, I_o; s, \gamma_R, \mu, N_D, N_A, \epsilon)$$

where the experimentally controlled variables are

k_g = grating wave number

E_0 = applied field (normal to grating planes)

λ = wavelength of incident light

T = temperature

I_0 = total irradiance

while the material parameters are

r = effective electro-optic coefficient

s = photoionization cross-section

γ_R = two-body recombination rate

μ = mobility

N_D = number of donors under dark conditions

N_A = number of traps under dark conditions

ϵ = static dielectric constant

n = background refractive index.

These equations were applied to cerium doped SBN in earlier work. Specifically, the sample contained 10^{19} cm^{-3} cerium atoms which resulted in an as-grown crystal with the following photorefractive parameters:

Γ = 11 cm^{-1}

τ_e = 0.10 s

α = 1.8 cm^{-1}

at

I_0 = 1W/cm^2

T = 298K

λ = 0.5145 μm

E_0 = 0 V/cm

λ_g = 5 μm

Variations in Γ and τ about this operating point are shown in Figs. 4 to 10. With no applied field, Fig. 4 indicates that Γ should be greater than 1 cm^{-1} for all practical values of λ_g, while the application of an electric field of 2 kV/cm ought to increase the coupling coefficient to 35 cm^{-1} at $\lambda_g = 5$ μm, as shown in Fig. 5. Such a large response would then make even very thin samples of SBN:Ce useful photorefractive media. However, in practice, these large values of Γ are not easily obtainable. As an electric field is applied to the crystal, induced stresses deform the material and the incident beams are distorted. Therefore, we conclude that the application of an electric field to the crystal in order to control its two-beam coupling coefficient is of limited use at this point.

Another manner in which Γ can be modified was suggested in Ref. (4). By varying the trap density N_A with reduction and oxidation treatments, one should be able to control Γ as shown in Fig. 6. Although the exact number density of traps is difficult to measure, we have indeed been able to change the two-beam coupling coefficient from less than 0.1 cm^{-1} to 15 cm^{-1} by heating the crystal in atmospheres with different oxygen partial pressures. However, the predicted variation of response time with trap density, which is shown in Fig. 7, has yet to be observed in SBN:Ce. Although Γ decreases as expected when the crystal is heated in a reducing atmosphere, the time constant remains unchanged at a typical value of 100 msec at 1 W/cm^2 irradiance. This unexpected and currently unexplained result has complicated our efforts at producing a cerium doped SBN photorefractive crystal with 1 millisecond response time, since heat treatment was proposed as a method of achieving this goal.[4] Therefore, other techniques may need to be invoked to obtain the desired speed of response.

Figures 8, 9 and 10 show how the response time τ is affected with changes in the mobility μ, the two-beam recombination rate γ_R, and the photoionization cross-section S, respectively. Since μ is predominantly an intrinsic quantity of the host crystal, little can be done to increase its value. However, S and γ_R are extrinsic parameters which can be varied by the selection of different dopants. By choosing a dopant with either a larger photoionization cross-section or a smaller two-body recombination rate coefficient than is presently obtained with cerium, the resulting doped sample of SBN should then

possess a shorter response time. The selection of such a dopant, unfortunately, is a nontrivial task.

Consider Table 8 which shows the results of an elemental analysis by nuclear activation of undoped and cerium doped SBN. Since undoped SBN is photorefractive[3] while containing only trace quantities of cerium, we must conclude that cerium is not the only photorefractive species for SBN. In fact, Table 8 indicates that significant amounts of Fe, Ni, Mo and Ta impurities are present in the undoped SBN crystal; Fe and Ni, for example, are known to be effective photorefractive centers in $LiNbO_3$.[9] Although iron has already been used as a dopant for SBN, the resulting crystals are optically imperfect. Therefore, we suggest that not only should the development of iron and cerium-doped SBN continue, but that crystals doped with other impuriries, which may prove to have better values of γ_R and S, should also be investigated.

The growth of SBN with different dopants is a method we now suggest as a means of improving the response time. Since our last report, the reduction of cerium doped SBN was accomplished, but with little effect on τ. However, this treatment was shown to vary the two-beam coupling coefficient considerably. The increases in Γ with the application of an electric field were marred by the unexpected distortions of the crystal induced by the field. Finally, the growth of SBN with varying concentrations of cerium proved that optically excellent samples of photorefractive SBN:Ce can now be readily produced.
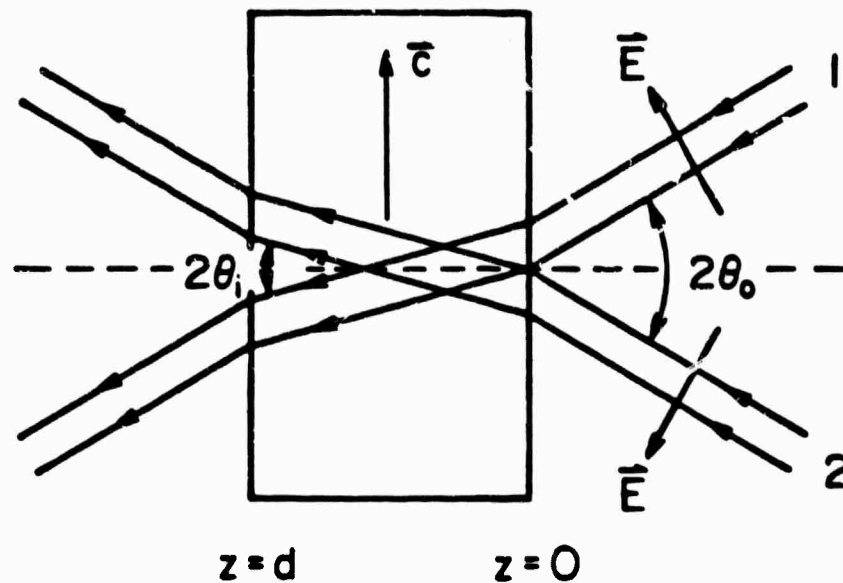
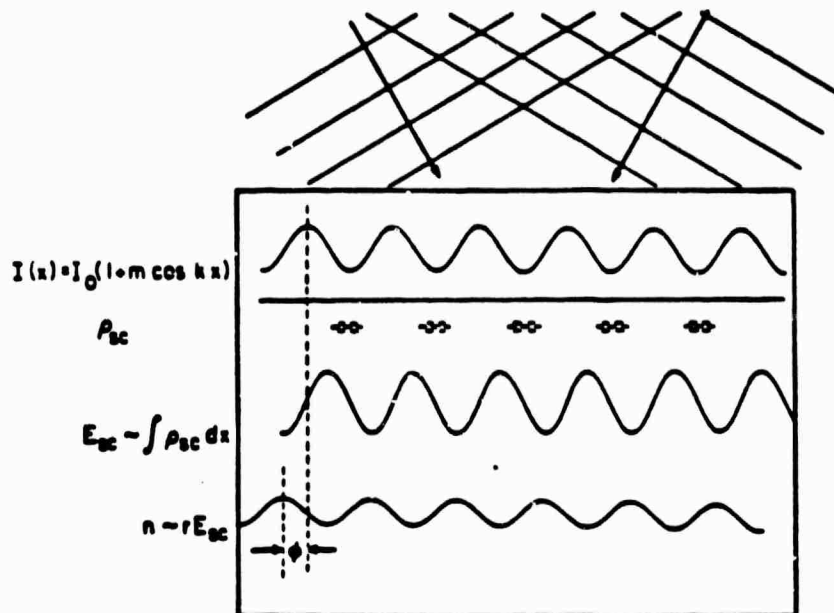Fig. 2 Experimental setup for two-beam coupling experiments.

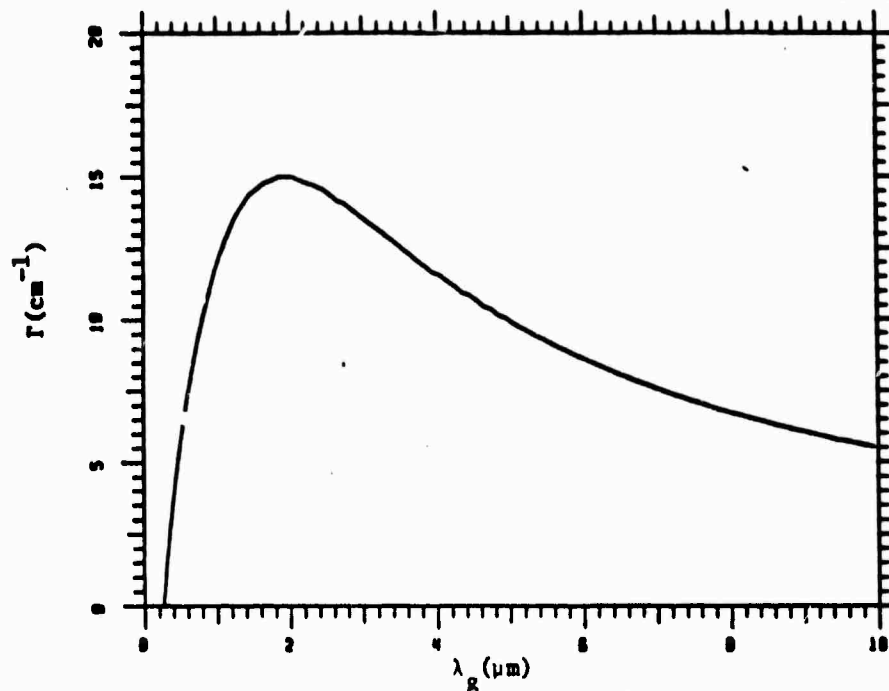Fig. 3 The photorefractive mechanism.

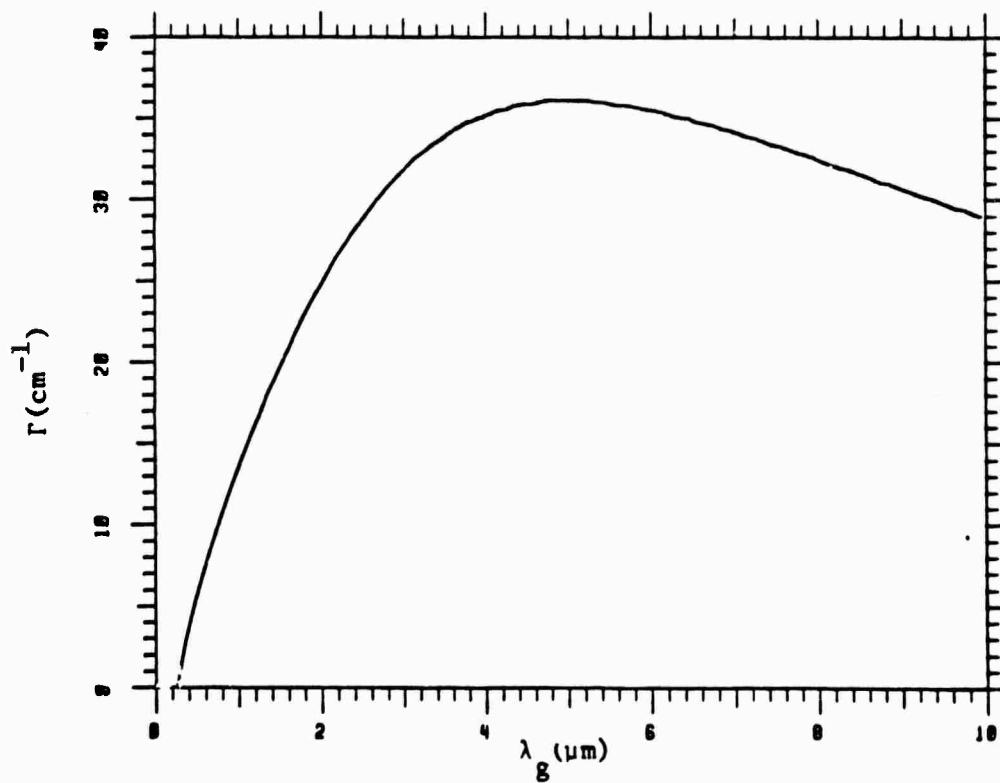Fig. 4 Coupling coefficient vs grating wavelength for E_0 = 0 V/cm.

Fig. 5 Coupling coefficient vs grating wavelength for E_0 = 2 kV/cm.
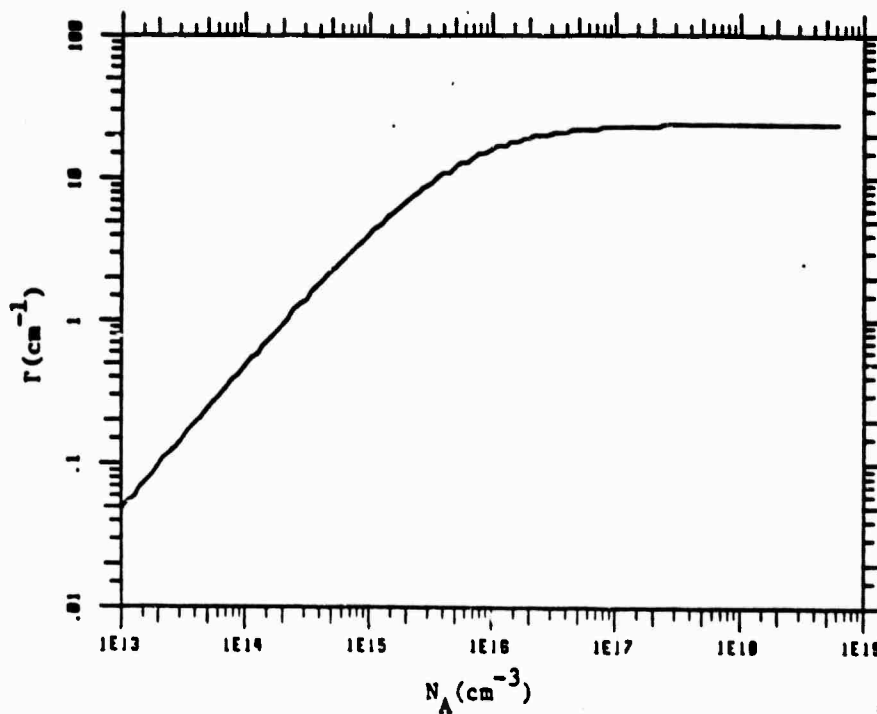
Fig. 6 Coupling coefficient vs acceptor trap density.
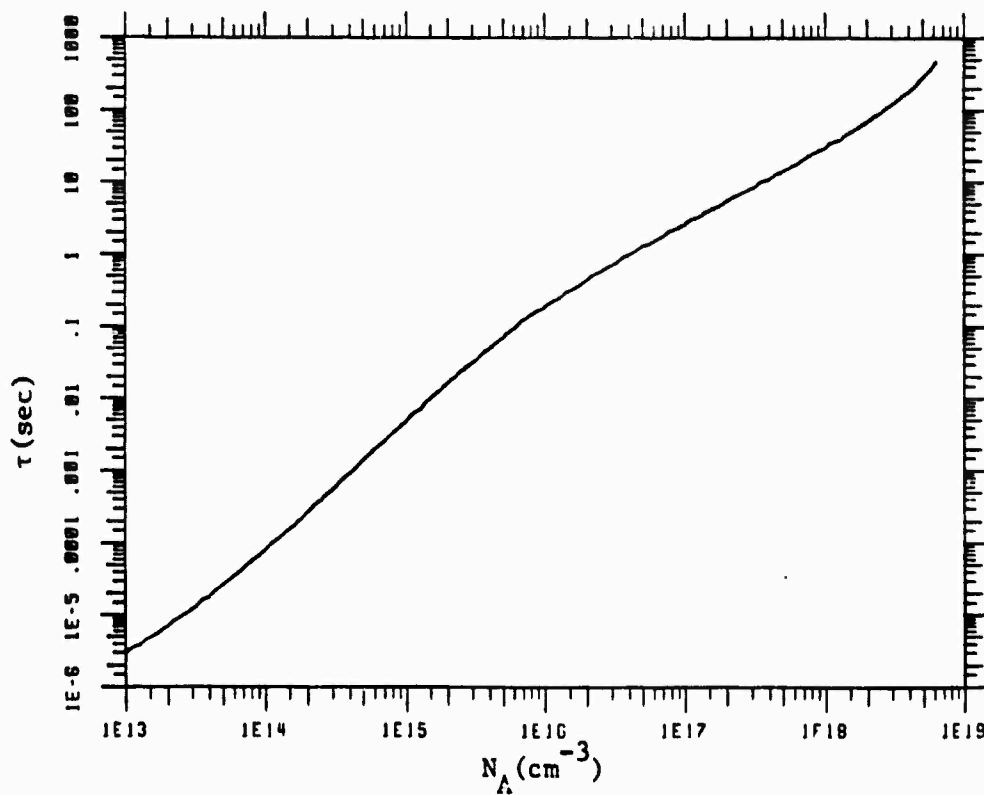

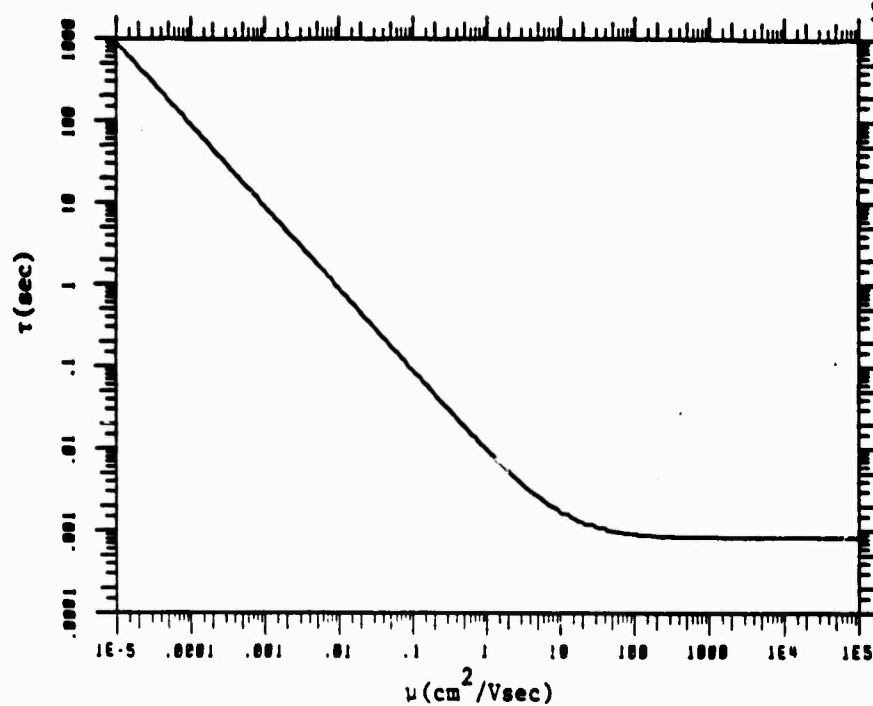Fig. 7 Response time vs. acceptor trap density.

Fig. 8   Response time vs electron mobility.
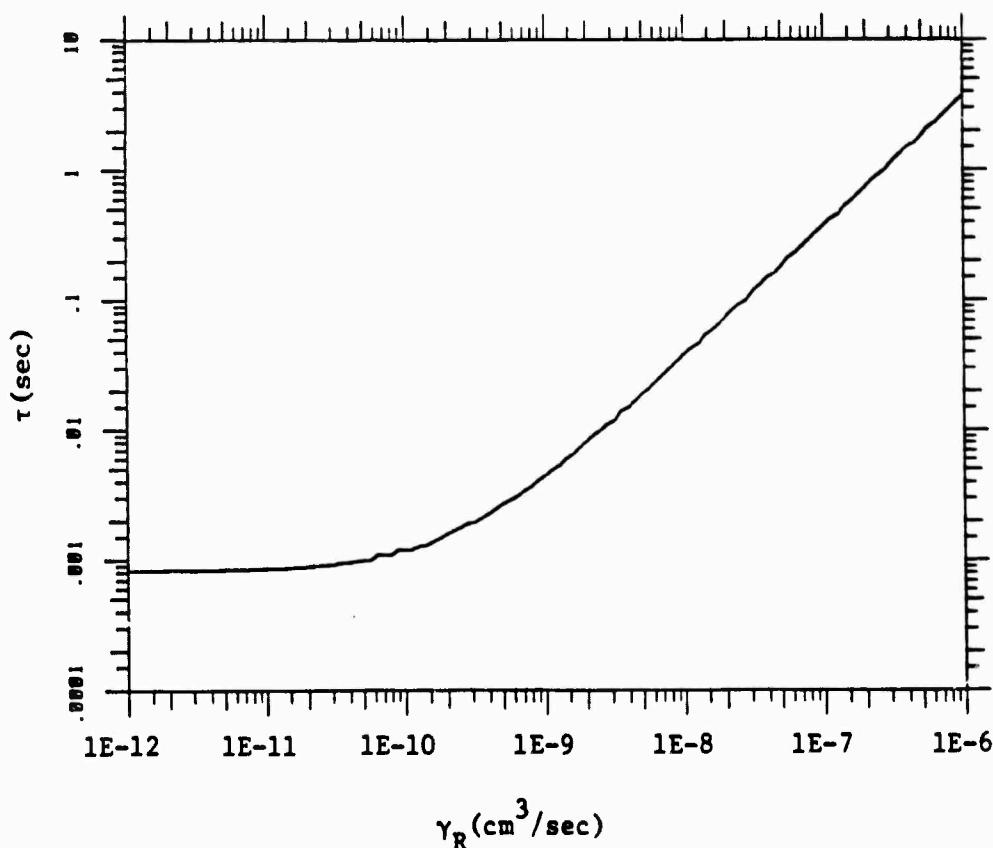
Fig. 9   Response time vs two-body recombination rate coefficient.
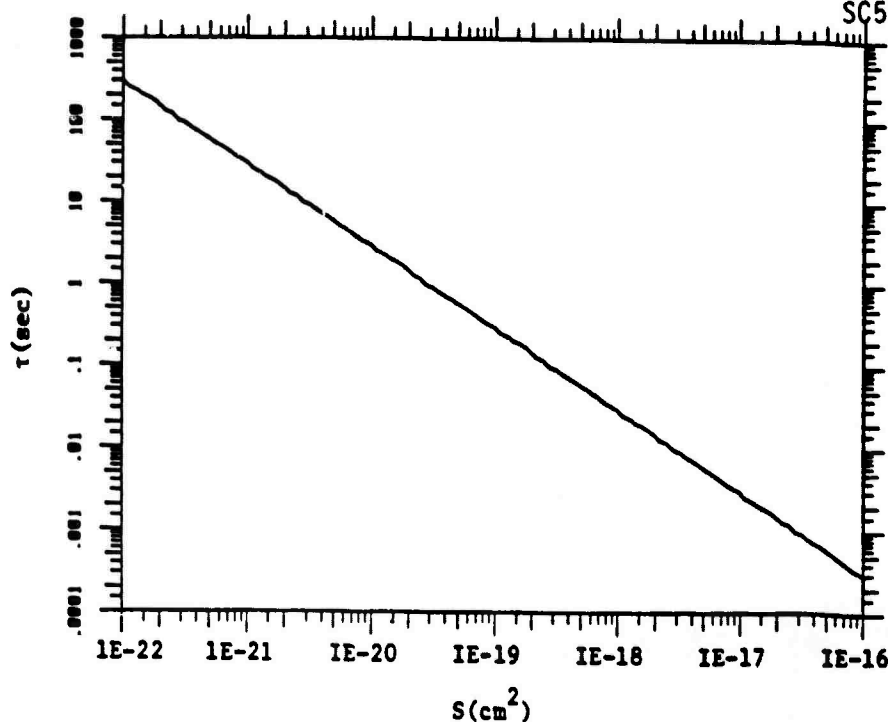
Fig. 10 Response time vs photoionization cross-section.

Table 8

Elemental Analysis by Weight of SBN and SBN:Ce

ELEMENT & UNITS	SBN**	SBN:CE**
U PPM	<0.1	<0.1
TH PPM	<0.3	<0.2
NA PPM	30	<30
SC PPM	0.04	0.03
CR PPM	<5.0	<5.0
FE %	0.029	0.014
CO PPM	0.3	0.3
NI PPM	50	50
IN PPM	7	5
AS PPM	<1	<1
SE PPM	<5.0	<5.0
BR PPM	<0.5	<0.5
MO PPM	11	4
SB PPM	0.5	0.5
CS PPM	<0.2	<0.2
BA PPM	160000	150000
LA PPM	0.2	1.0
HF PPM	<0.2	<0.2
TA PPM	12	13
W PPM	<3	1
AU PPB	<5	5
CE PPM	<1	47
ND PPM	INTERFER	INTERFER
SM PPM	0.01	0.32
EU PPM	0.07	0.10
TB PPM	<0.1	<0.1
YB PPM	<0.05	0.05
LU PPM	<0.01	<0.01
SR PPM	148000	135000
RB PPM	<5	<5

4.0 FUTURE PLANNED WORK

- Further refine and evaluate the growth of high purity SBN:50 and SBN:60 single crystals.

- Continue development of Fe- and Ce-doped SBN:60, and attempt to establish the dopant valence states using optical spectroscopy and other analytical techniques.

- Investigate the dielectric and optical properties of SBN:60 doped with other cations such as Cr^{3+}, Co^{2+}/Co^{3+}, etc.

- Establish the pyroelectric figure-of-merit for tungsten bronze ferroelectric compositions using the crystal chemical approach.

- Continue measurement of the E-O coefficients for near-morphotropic single crystal PBN.

- Continue to evaluate photorefractive properties, specifically sensitivity and speed, using two- and four-wave mixing techniques.

5.0 PUBLICATIONS AND PRESENTATIONS

5.1 Publications

1. R.R. Neurgaonkar, W.K. Cory and J.R. Oliver, "Growth and Applications of Ferroelectric Tungsten Bronze Family Crystals," Ferroelectrics <u>51</u>, 3 (1983).

2. R.R. Neurgaonkar, J.R. Oliver and L.E. Cross, "Ferroelectric Properties of Tetragonal Tungsten Bronze Single Crystals," Ferroelectrics <u>56</u>, 31 (1984).

3. T.R. Shrout, L.E. Cross and D.A. Hukin, "Ferroelectric Properties of Tungsten Bronze Lead Barium Niobate (PBN) Single Crystals."

4. R.R. Neurgaonkar and L.E. Cross, "Piezoelectric Tungsten Bronze Crystals for SAW Applications," submitted to Mat. Res. Bull.

5. R.R. Neurgaonkar, W.K. Cory and J.R. Oliver, "Growth and Applications of T-B Family Crystals," accepted Proc. Southwest Optics Symposium.

6. R.R. Neurgaonkar, W.K. Cory and J.R. Oliver, "Growth of Tungsten Bronze Ferroelectric KLN Crystals," submitted to J. Cryst. Growth.

5.2 Presentations

1. R.R. Neurgaonkar, W.K. Cory and J.R. Oliver, "Growth and Applications of Tungsten Bronze Family Crystals," presented at the 1983 IEEE Int. Symp. on Applications of Ferroelectrics, June 1-3, 1983, Gaithersburg, MD.

2. R.R. Neurgaonkar, J.R. Oliver and L.E. Cross, "Growth and Application of Ferroelectric Tungsten Bronze Family Crystals," presented at the 5th European Meeting on Ferroelectrics, Sept. 26-30, 1983, Benalmadena, Spain.

3. T.R. Shrout, H.C. Chen and L.E. Cross, "Dielectric and Piezoelectric Properties of Tungsten Bronze Lead Barium Niobate ($Pb_{1-x}Ba_xNb_2O_6$) Single Crystals," presented at the 5th European Meeting on Ferroelectrics, Sept. 26-30, 1983, Benalmadena, Spain.

4. J.R. Oliver and R.R. Neurgaonkar, "Ferroelectric Solid Solutions Based on the Tungsten Bronze Structure," presented at the 86th Annual Meeting of the Am. Ceram. Soc., April 30-18, 1984, Pittsburgh, PA (invited paper).

5. J.R. Oliver and R.R. Neurgaonkar, "Morphotropic Tungsten Bronze Solid Solutions," presented at the 37th Pacific Coast Regional Meeting of the Am. Ceram. Soc., October 28-31, 1984, San Francisco, CA.

6.   R.R. Neurgaonkar, W.K. Cory and J.R. Oliver, "Ferroelectric Tetragonal Tungsten Bronze Crystals for Optoelectronic Applications," presented at the 37th Pacific Coast Regional Meeting of the Am. Ceram. Soc., October 28-31, 1984, San Francisco, CA.

7.   R.R. Neurgaonkar, W.K. Cory and J.R. Oliver, "Growth and Applications of T.B. Bronze Family Crystals," presented at the Southwest Optics Symposium, Albuquerque, NM, March 2-8, 1985.

6.0 REFERENCES

1. K. Megumi, H. Kozuka, M. Kobayashi and Y. Furuhata, Appl. Phys. Lett. <u>30</u>, 631 (1977).

2. S.T. Liu and M.J. Maciolek, J. Electronic Mat. <u>4</u>, 91 (1975).

3. G.A. Rakuljic, A. Yariv, and R.R. Neurgaonkar, "A Comparative Evaluation of the Photorefractive Effect in $Sr_{.6} Ba_{.4}Nb_2O_6$ (SBN) SBN:Fe, and SBN:Ce by Two-Beam Coupling," (1984).

4. G.A. Rakuljic, A. Yariv, and R.R. Neurgaonkar, "Application of the Band Transport Model to Photorefractive Strontium Barium Niobate," (1984).

5. G.C. Valley and M.B. Klein, Opt. Eng. <u>22</u>, 6, 704 (1983).

6. N.V. Kukhtarev, V.B. Markov, and S.G. Odulov, Opt. Comm. <u>23</u>, 338 (1977).

7. N.V. Kukhtarev, V.B. Markov, S.G. Odulov, M.S. Soskin and V.L. Vinetskii, Ferroelectrics <u>22</u>, 949 (1979).

8. N.V. Kukhtarev, Sov. Tech. Phys. Lett. <u>2</u>, 438 (1976).

9. W. Phillips, J.J. Amodei, and D.L. Staebler, RCA Review <u>33</u>, 94 (1972).

APPENDIX

A PHENOMENOLOGICAL ANALYSIS OF TETRAGONAL TUNGSTEN BRONZE FERROELECTRICS

L.E. Cross
Materials Research Laboratory
The Pennsylvania State University
University Park, PA   16802

R.R. Neurgaonkar
Rockwell International Science Center
Thousand Oaks, CA   91360

ABSTRACT

A simple Devonshire form has been derived for the Phenomenological Elastic Gibbs Function to describe the elasto-dielectric parameters of simple proper ferroelectrics in the tungsten bronze structure family which has 4/mmm prototypic point symmetry. For the assumption that all temperature dependence is carried by the Curie-Weiss behavior implicit in the quadratic term and that the expansion may be terminated at the first 6th order term, reasonable agreement between calculated and derived P_S vs. T curves in the ferroelectric phase can be obtained for a wide range of bronze compositions.

From the fitting it is clear that second and sixth rank terms are remarkably constant over a very wide range of bronze compositions. Variation in the negative fourth rank term is larger, but this is to be expected since it contains large contributions from electrostrictive and elastic terms which will depend upon boundary conditions.

These initial studies suggest that the phenomenological method may be used to derive expectation values for tensor parameters across the whole family of ferroelectric bronzes. The study also points up the need for more careful detailed studies of lattice strain, birefringence and permittivity as a function of temperature in model bronze compounds to provide more detailed checks of the method.

1.0 INTRODUCTION

The tungsten bronze family of simple proper ferroelectrics incorporates now almost 100 different end member compositions, most of which are mutually compatible in solid solution, so that an immense range of possible ferroelectrics is now available. In attempting to select compositions for device application in optics, nonlinear optics, electro-optics, acousto-optics, SAW, etc., it is important for each device to maximize a different combination of the tensor properties of the crystal, so that some theoretical predictive capability would be of major help in making rational choices in this bewildering range of possible bronze compositions. For complex structures like the ferroelectric bronzes, however, where different cations can have different fractional occupancy on several sites in the structure, a rigorous atomistic theory is, at present, out of the question. It is our purpose to explore the extent to which thermodynamic phenomenological methods can be used to correlate the tensor properties, point up the inadequacies of present experimental data, and suggest a more systematic experimental approach.

A rather simple Landau:Ginsburgh:Devonshire function for the Elastic Gibbs Free Energy of simple proper ferroelectric bronzes which can be derived for the 4/mmm prototype symmetry has been discussed earlier (1), and the function was used with good results to fit the dielectric, electric and piezoelectric properties of the $Sr_{0.60}Ba_{0.40}Nb_2O_6$ (SBN:60) ferroelectric composition (2). A simple power series expansion up to the first 6th power terms in polarization, but including only fourth rank terms in elastic and elasto-electric coupling terms, proved adequate to explain dielectric, piezoelectric and spontaneous shape change data; however, it was necessary to include sixth order electrostriction to model the elastic constant behavior. The relaxor dielectric character of SBN was taken into account by using a narrow distribution of Curie temperatures T_c, and did not obtrude in the fitting process except for properties very close to $\overline{T}_c$ where fluctuations in the polarization take $\overline{P}_3^2$ far from zero (3).

2.0 THERMODYNAMIC PHENOMENOLOGY

Recapitulating our earlier studies, it has been the contention that an empirical thermodynamic elastic Gibbs function can be developed which will describe the polarization induced changes in the dielectric, elastic, thermal, piezoelectric and electro-optic properties in all possible simple proper ferroelectric phases of the tungsten bronze structure ferroelectrics.

Under the symmetry constraints of the 4/mm point symmetry for the prototypic form of the bronzes, the permitted dielectric stiffnesses α_{ij}, fourth order stiffnesses α_{ijkl}, electrostriction constants Q_{ijkl}, elastic compliances s_{ijkl}, and sixth order dielectric stiffnesses α_{ijklmn} are listed in Tables I through IV.

Using the reduced notation 11 -> 1, 22 -> 2, 33 -> 3, 23 or 32 -> 4, 13 or 31 -> 5 and 12 or 21 -> 6 the elastic Gibbs function takes the form

$$
\Delta G_1 = \alpha_1(P_1^2+P_2^2) + \alpha_3 P_3^2 + \alpha_{11}(P_1^4+P_2^4) + \alpha_{33}P_3^4 \tag{1}
$$

$$
+ \alpha_{13}(P_1^2 P_3^2+P_2^2 P_3^2) + \alpha_{12}P_1^2 P_2^2 + \alpha_{333}P_3^6
$$

$$
+ \alpha_{111}(P_1^6+P_2^6) - \frac{1}{2} s_{11}(X_1^2+X_2^2) - s_{12}X_1 X_2
$$

$$
- s_{13}(X_1+X_2)X_3 - \frac{1}{2} s_{33}X_3^2 - \frac{1}{2} s_{44}(X_4^2+X_5^2)
$$

$$
- \frac{1}{2} s_{66}S_6^2 - Q_{11}(P_1^2 X_1+P_2^2 X_2) - Q_{12}(P_1^2 X_2+P_2^2 X_1)
$$

$$
- Q_{13}(P_1^2 X_3+P_2^2 X_3) - Q_{31}(P_3^2 X_1+P_3^2 X_2)
$$

$$
- Q_{33}P_3^2 X_3 - Q_{44}(P_2 P_3 X_4+P_1 P_3 X_5)
$$

$$
- Q_{66}P_1 P_2 X_6
$$

The first partial derivatives with respect to the polarization give the field components

$$\frac{\partial \Delta G}{\partial P_1} = E_1 \, 2a_1 P_1 + 4a_{11} P_1^3 + 2a_{13} P_1 P_3^2$$

$$+ 2a_{12} P_1 P_2^2 + 6a_{111} P_1^5$$

$$+ Q_{13} P_1 X_3 + Q_{44} P_3 X_5 + Q_{66} P_1 X_6 \qquad (2)$$

$$\frac{\partial \Delta G}{\partial P_2} = E_2 = 2a_1 P_2 + 4a_{11} P_2^3 + 2a_{13} P_2 P_3^2$$

$$+ 2a_{12} P_2 P_1^2 + 6a_{111} P_2^5$$

$$+ 2Q_{13} P_2 X_3 + Q_{44} P_3 X_4 + Q_{66} P_1 X_6 \qquad (3)$$

$$\frac{\partial \Delta G}{\partial P_3} = E_3 = 2a_3 P_3 + 4a_{33} P_3^3 + 2a_{13} (P_1^2 + P_2^2) P_3$$

$$+ 6a_{33} P_3^5 + 2Q_{31} P_3 (X_1 + X_2)$$

$$+ 2Q_{33} P_3 X_3 + Q_{44} (P_2 X_4 + P_1 X_5) \qquad (4)$$

It is the solutions of these equations with $E_i = 0$ which determine the ferroelectric states for a free crystal ($X = 0$). In general, there are seven possible ferroelectric species which can occur from the prototypic 4/mmm symmetry of the paraelectric phase of the tungsten bronze, each of which corresponds to a different combination of non-zero (spontaneous) values of the P_i components. All possible solutions for the three equations (2-4) were derived and reported by Cross and Pohanka (1968). Practically, however, just two of these solutions encompass all presently known simple ferroelectric bronzes. These are

(a) $P_3^2 \neq 0$ $\quad\quad$ $P_1 = P_2 = 0$

(b) $P_1^2 = P_2^2 \neq 0$ $\quad\quad$ $P_3 = 0$.

The species (a) corresponds to the Shuvalov (1970) species 4/mmm (1) D4 F4mm, where 4/mmm is the high temperature prototype point group and F4mm means that the crystal is ferroelectric of point group 4mm below the transition temperature. D(4) indicates that the spontaneous polarization P_s has definite orientation along the four-fold symmetry axes, and (1) denotes number of equivalent four-fold axes which is one. In other words, there are two domains of opposite orientation of P_s (I.E., 180° domains) along the four-fold prototypic axis. The second species (b) is one of the subtypes of 4/mmm (2)D2 Fmm2 with P_s along the two-fold axis which make angles of 45° with the 1 and 2 prototype axis ($P_1^2 = P_2^2$) and has four equivalent ferroelectric domain states.

Substituting the conditions (a) into the general equations (2-4) gives the following conditions for stability:

$$P_1 = P_2 = 0 \quad\quad 0 = 2\alpha_3 + 4\alpha_{33}P_3^2 + 6\alpha_{333}P_3^4 \tag{5}$$

The isothermal dielectric stiffness χ are

$$\chi_{11}^T = 2\alpha_1 + 2\alpha_{13}P_3^2$$
$$\chi_{22}^T = 2\alpha_1 + 2\alpha_{13}P_3^2$$
$$\chi_{33}^T = 2\alpha_3 + 12\alpha_{33}P_3^2 + 30\alpha_{333}P_3^4$$
$$\chi_{12}^T = \chi_{13}^T = \chi_{23}^T = 0 \tag{6}$$

The tetragonal spontaneous strains are given by

$$x_1 = Q_{31}P_3^2 \quad\quad x_4 = x_5 + x_6 = 0$$
$$x_2 = Q_{31}P_3^2$$
$$x_3 = Q_{33}P_3^2 \tag{7}$$

and the piezoelectric b coefficients by

$$b_{11} = 0 \qquad b_{21} = 0 \qquad b_{31} = 2Q_{31}P_3$$

$$b_{12} = 0 \qquad b_{22} = 0 \qquad b_{32} = 2Q_{31}F_3$$

$$b_{13} = 0 \qquad b_{23} = 0 \qquad b_{33} = 2Q_{33}P_3$$

$$b_{14} = 0 \qquad b_{24} = Q_{44}P_3 \qquad b_{44} = 0$$

$$b_{15} = Q_{44}P_3 \qquad b_{25} = 0 \qquad b_{35} = 0$$

$$b_{16} = 0 \qquad b_{26} = 0 \qquad b_{36} = 0 \qquad\qquad (8)$$

For the case (b) the corresponding equations take the form, for the stability conditions,

$$P_1^2 = P_2^2 \qquad 0 = 2a_1 + (4a_{11} + 2a_{12})P_1^2 + 6a_{111}P_1^4$$

$$P_3 = 0 \qquad\qquad (9)$$

The isothermal stiffnesses are

$$X_{11}^T = 2a_1 + 12a_{11}P_1^2 + 2a_{12}P_1^2 + 30a_{111}P_1^4$$

$$X_{22}^T = 2a_1 + 12a_{11}P_1^2 + 2a_{12}P_1^2 + 30a_{111}P_1^4$$

$$X_{33}^T = 2a_3 + 4a_{13}P_1^2$$

$$X_{34}^T = 4a_{12}P_1^2 \qquad X_{13} = X_{23} = 0 \qquad\qquad (10)$$

It may be noted that the coefficients here are expressed with respect to the original prototypic axes and thus satisfy pseudomonoclinic symmetry. However, a simple rotation of the matrix by 45° in the 1, 2 plane would reveal the true orthorhombic symmetry.

Spontaneous elastic strains take the form

$$x_1 = (Q_{11}+Q_{12})P_1^2$$
$$x_2 = (Q_{11}+Q_{12})P_1^2$$
$$x_3 = 2Q_{13}P_1^2$$
$$x_6 = Q_{66}P_1^2 \qquad x_4 = x_5 = 0 \tag{11}$$

and the piezoelectric coefficients are

$$
\begin{array}{lll}
b_{11} = 2Q_{11}P_1 & b_{21} = 2Q_{12}P_1 & b_{31} = 0 \\
b_{12} = 2Q_{12}P_1 & b_{22} = 2Q_{12}P_1 & b_{32} = 0 \\
b_{13} = 2Q_{13}P_1 & b_{23} = 2Q_{13}P_1 & b_{33} = 0 \\
b_{14} = 0 & b_{24} = 0 & b_{34} = Q_{44}P_1 \\
b_{15} = 0 & b_{25} = 0 & b_{35} = Q_{44}P_1 \\
b_{16} = Q_{66}P_1 & b_{26} = Q_{66}P_1 & b_{36} = 0
\end{array} \tag{12}
$$

Table 1

Equivalent Second and Fourth Rank Dielectric Terms for 4/mmm Symmetry

Nye's Matrix Notation		Full Tensor Notation		Number of Equivalent Terms
Term	Symmetry Equivalent Terms	Term	Symmetry Equivalent Terms	
α_1	α_2	α_{11}	α_{22}	2
α_3		α_{33}		1
α_{11}	α_{22}	α_{1111}	α_{2222}	2
α_{12}	α_{21}, α_{66}	α_{1122}	α_{1212}, α_{1221}, α_{2112}, α_{2121}, α_{2211}	
α_{13}	α_{31}, α_{23}, α_{32}, α_{44}, α_{55} ($\alpha_{44} = 4\alpha_{2323}$)	α_{1133}	α_{3311}, α_{2233}, α_{1313}, α_{1313}, α_{1331}, α_{3113}, α_{3131}, α_{2323}, α_{2332}, α_{3223}, α_{3232}	12
α_{33}		α_{3333}		1

Table II

Equivalent Electrostriction Terms for 4/mmm Symmetry

| Nye's Matrix Notation | | Full Tensor Notation | | Number of |
Term	Symmetry Equivalent Terms	Term	Symmetry Equivalent Terms	Equivalent Terms
Q_{11}	Q_{22}	Q_{1111}	Q_{2222}	2
Q_{12}	Q_{21}	Q_{1122}	Q_{2211}	2
Q_{13}	Q_{23}	Q_{1133}	Q_{2233}	2
Q_{31}	Q_{32}	Q_{3311}	Q_{3322}	2
Q_{33}		Q_{3333}		1
Q_{44}	Q_{45}	Q_{2323}	Q_{2332}, Q_{3223}, Q_{3232}, Q_{1313}, Q_{1331}, Q_{8113}, Q_{3151}	8
Q_{66}		Q_{1212}	Q_{1221}, Q_{2112}, Q_{2121}	4

Table III

Equivalent Elastic Compliance Terms for 4/mmm Symmetry

| Nye's Matrix Notation | | Full Tensor Notation | | Number of |
Term	Symmetry Equivalent Terms	Term	Symmetry Equivalent Terms	Equivalent Terms
s_{11}	s_{22}	s_{1111}	s_{2222}	2
s_{12}	s_{21}	s_{1122}	s_{2211}	2
s_{13}	s , s_{23}, s_{32}	s_{1133}	s_{3311}, s_{2233}, s_{3322}	4
s_{33}		s_{3333}		1
s_{44}	s_{55}	s_{2323}	s_{2332}, s_{3223}, s_{3232}, s_{1313}, s_{1331}, s_{3113}, s_{3131}	8
s_{66}		s_{1212}	s_{1221}, s_{2112}, s_{2121}	4

Table IV

Equivalent Sixth Rank Tensor Terms of the Form $\alpha(P^6)$
for 4/mmm Symmetry

	Term	Symmetry Related Terms	Number of Equivalent Terms
1.	α_{111}	222	2
2.	α_{112}	166, 121, 616, 661, 211, 221, 266, 212, 626. 662, 122	30
3.	α_{113}	155, 131, 515, 551, 331, 223, 244, 232, 424, 442, 322	30
4.	α_{123}	144, 132, 525, 645, 546, 636, 663, 564, 654, 552, 321, 441, 231, 465, 366, 255, 456, 213, 414, 312	90
5.	α_{133}	535, 553, 331, 355, 313, 233, 434, 443, 332, 344, 323	30
6.	α_{333}		1

3.0 POTENTIAL UTILITY OF THE PHENOMENOLOGICAL THEORY

3.1 Introduction

It is evident from Tables I through IV that a substantial number of constants are required to characterize the bronzes in this phenomenological manner. The only formal benefit is that all the elasto-dielectric parameters of the lower symmetry ferroelectric forms can be characterized in terms of the nonlinear parameters of the higher symmetry prototype form.

In principle, it is possible that all the parameters can be functions of both temperature and composition. However, several pieces of evidence, both direct and indirect suggest that:

(a) The dominant temperature dependence is carried in the terms α_1 and α_3 which have a Curie-Weiss form

$$\alpha_1 = \alpha_{10} \, (T-\theta_1)$$
$$a_3 = \alpha_{30} \, (T-\theta_3) \tag{13}$$

(b) The higher order constants do not change markedly with either temperature or composition across a wide field of compounds and solid solutions with the bronze structure.

In earlier studies we have demonstrated

1. That in all known ferroelectric bronzes, only two of the seven possible ferroelectric species which are available from the 4/mmm prototype occur in nature.

2. In the tetragonal ferroelectric form in $(Sr_{0.61}Ba_{0.39})Nb_2O_6$, which is the congruently melting SBN composition, the data followed very closely to the phenomenology except for temperatures close to the Curie point T_c, and all parameters have been evaluated.

3. For the $(Pb_{1-x}Ba_x)Nb_2O_6$ compositions in the tetragonal phase field, but close to the morphotropic phase boundary at the $(Pb_{0.6}Ba_{0.4})Nb_2O_6$ composition, the dielectric, piezoelectric and electro-optic behavior can be quite accurately modeled using the phenomenological constants for SBN and just adjusting Θ_1 and Q_3 to conform to the observed Curie-Weiss behavior in these compositions.[4]

The success to date with the modeling suggest that we attempt a more ambitious assessment of the range of validity of our simple hypotheses (a) and (b) above using a much wider range of bronze compounds and making use of literature values to evaluate directly, wherever possible, the stiffness parameters. The results of this effort will form the bulk of this paper.

A second feature which has become evident from our modeling of the tungsten bronze ferroelectrics is that particularly in the elastic response, the relaxor character of the bronzes is reflected in a breakdown of the static phenomenological model at temperatures close to T_c due to the onset of fluctuations in P. Thus for a range of temperatures above T_c, it is evident that even though $\overline{P} = 0$, it is rigorously true that $\overline{P}^2 \neq 0$. The onset of a substantial fluctuating component in P will clearly affect all parameters which depend on even powers of P, such as the linear dimensions, since

$$x_{ij} = Q_{ij33}P_3^2 \tag{14}$$

as well as the optical refractive index given by

$$\Delta B_{ij} = g_{ij33}P_3^2 \tag{15}$$

and the elastic compliance

$$s_{ijkl} = \phi_{ijkl33}P_3^2 \tag{16}$$

Perhaps the easiest to analyze is the strain response, and this will be the subject of a subsequent paper.

3.2 Evaluation of the Thermodynamic Parameters

In spite of the fact that more than 100 different ferroelectric compounds with the tungsten bronze structure have been synthesized, and innumerable solid solutions can be made between these end member compositions, there is a genuine paucity of reliable experimental data from which to evaluate the thermodynamic constants. For many materials, only ceramic samples have been made and in these, it is impossible to separate the individual tensor components. Even in many systems where good single crystals have been grown, the headlong rush to print has left many of the important parameters unmeasured.

For this study we have been able to find adequate but incomplete data for several $Sr_{1-x}Ba_xNb_2O_6$ solid solutions. In several $La_2O_3:Sr_2KNb_5O_{15}$ compounds and solid solutions and for pure $Sr_2KNb_5O_{15}$ there are also adequate, though incomplete, data. $Ba_2NaNb_5O_{15}$ may be analysed on this model if the weak ferroelastic phase change near 370°C is neglected, and there are some data for a titanium modified $Ba_2NaNb_5O_{15}$. Similarly, in $K_3Li_2Nb_5O_{15}$ there are adequate data for some of the constants, though the transverse dielectric response has apparently not been measured.

In the orthohombic ferroelectric form, we have only been able to find data for $PbNb_2O_6$ and for $Pb_2KNb_5O_{15}$. The fitting to obtain the thermodynamic parameters is, however, more difficult in these compositions and will be covered in a subsequent paper.

For the tetragonal ferroelectric form, the evaluation is relatively straight-forward. The constant α_3 has the form $\alpha_3 = \alpha_{30}(T-\Theta_3)$ which leads to an equation for the stiffness χ_{33} above T_c of the form

$$\chi_{33} = 2\alpha_{30}(T-\theta_3) \tag{17}$$

Thus the extrapolation of the Curie Weiss plot of stiffness above T_c gives the temperature θ and the slope in the constant $2\alpha_{30}$.

By equating the ΔG values in ferroelectric and paraelectric states at T_c, the equation for P_s can be put into the Devonshire form

$$\frac{T-\theta}{T_0-\theta} - 4\left(\frac{P_3}{P_{30}}\right)^2 + 3\left(\frac{P_3}{P_{30}}\right)^4 = 0 \tag{18}$$

in which $T_c - \theta$ and P_{30} are the only fitting parameters. Often, unfortunately, the published P_s vs T data for ferroelectric crystals is unreliable, particularly at temperatures remote from T_c where it is often difficult to pole to a single domain state. Thus it is wise to check the shape of the polarization function by using a less direct method, e.g. the spontaneous strains $\Delta c/c$ and $\Delta a/a$ induced in the ferroelectric form are electrostrictive in nature and thus scale with P_s^2. The piezoelectric b_{ij} constants on the other hand, being morphic, scale directly with P_s as do the linear electro-optic effect and the nonlinear Miller δ coefficients.

A typical fitting of the different P_s data for $Ba_2NaNb_5O_{15}$ is shown in Fig. 1. Clearly the Devonshire form is in excellent agreement with the 'birefringence' data which are probably most reliable in this crystal. From the values of T_c, θ, P_{so} and χ_{30}, the α constants are given by

$$\alpha_3 = 1/2 \; \alpha_{30}(T_c - \theta_3) \tag{19}$$

$$\alpha_{33} = - \frac{\alpha_{30}(T_c - \theta_3)}{P_{so}} \tag{20}$$

$$\alpha_{333} = \frac{\alpha_{30}(T_c - \theta_3)}{2(P_{so})^4} \tag{21}$$

For the constant α_1 and α_{13}, dielectric data for a section parallel to the c axis (ϵ_a) is required. Above T_c,

so that $2\alpha_{10}$ is the Curie-Weiss slope and θ_1 is the extrapolated Curie temperature.

To derive α_{13} it is then a simple matter to make use of equation (10) to obtain, by the least squares method, a best fit to the experimental data below T_c, taking now calculated values for P_3 vs T. A typical plot comparing measured and calculated values for $Ba_2NaNb_5O_{15}$ is given in Fig. 2. Using these methods, constants for the bronze compositions derived are listed in Table V.

3.3   Discussion

It may be noted at once that for α_{30} and α_{333} there is excellent agreement over a very wide range of bronze compositions. The constant α_{10} is also within a narrow range, though here the stiffness is much larger and the Curie-Weiss slope more difficult to read precisely. The α_{33} values cover a wider range and this also is perhaps not surprising. In the elastic Gibbs function, the negative value of α_{33} comes about because of a strong contribution from elastic and electrostrictive constants in the free crystal. Thus the magnitude of α_{33} is markedly dependent on the elastic boundary conditions and probably therefore on the crystal perfection. The α_{13} values also cover a rather wider range, but here the error is probably in the evaluation.

In summary, it does appear from these preliminary data that the original hypothesis of a constancy of the higher order stiffnesses is a good approximation for the tetragonal bronze ferroelectrics, and thus can form a basis for the analysis of the properties of a very wide range of bronze compositions.
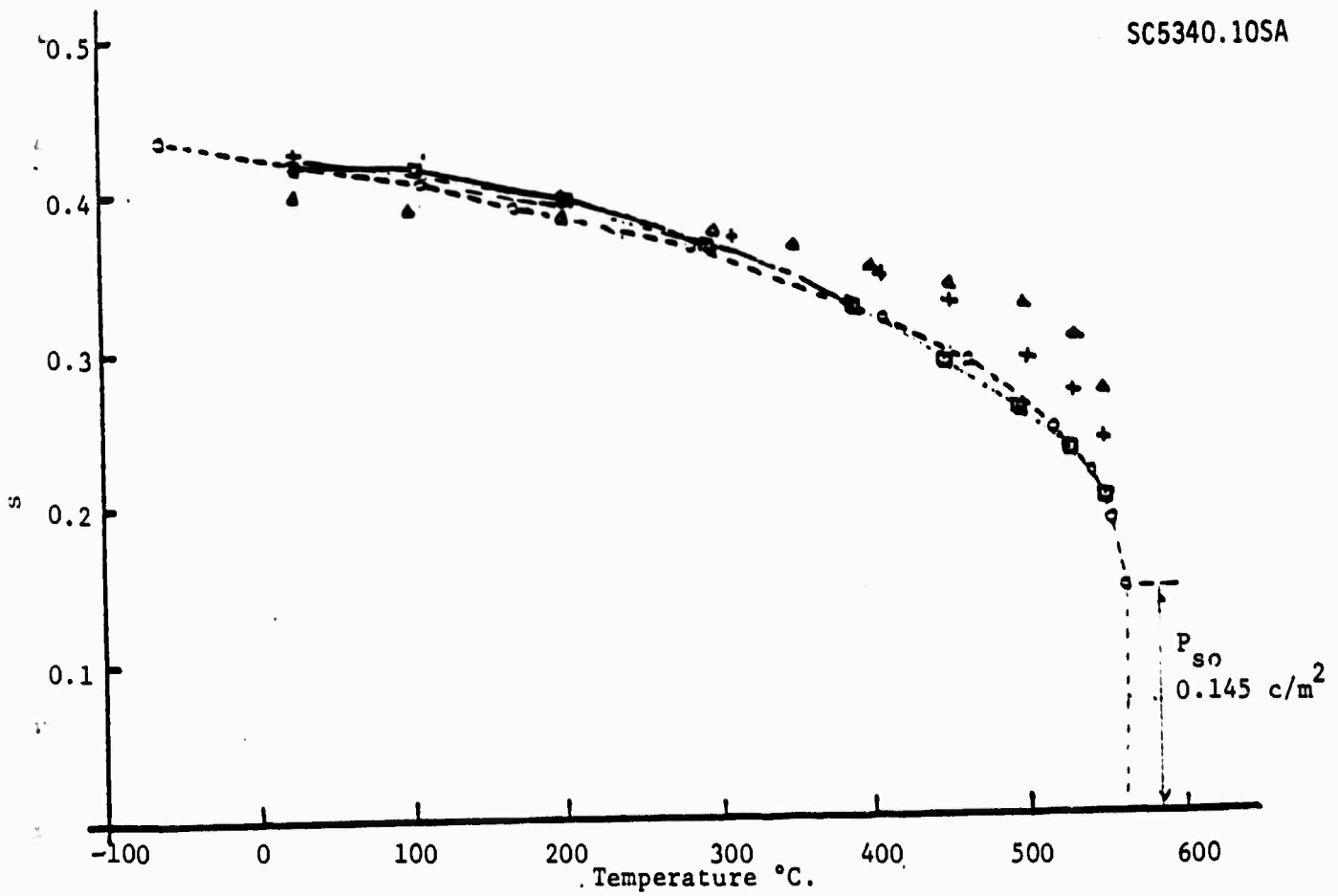
Figure 1.   Phenomenological fitting of P_s vs T in $NaBa_2Nb_5O_{15}$.

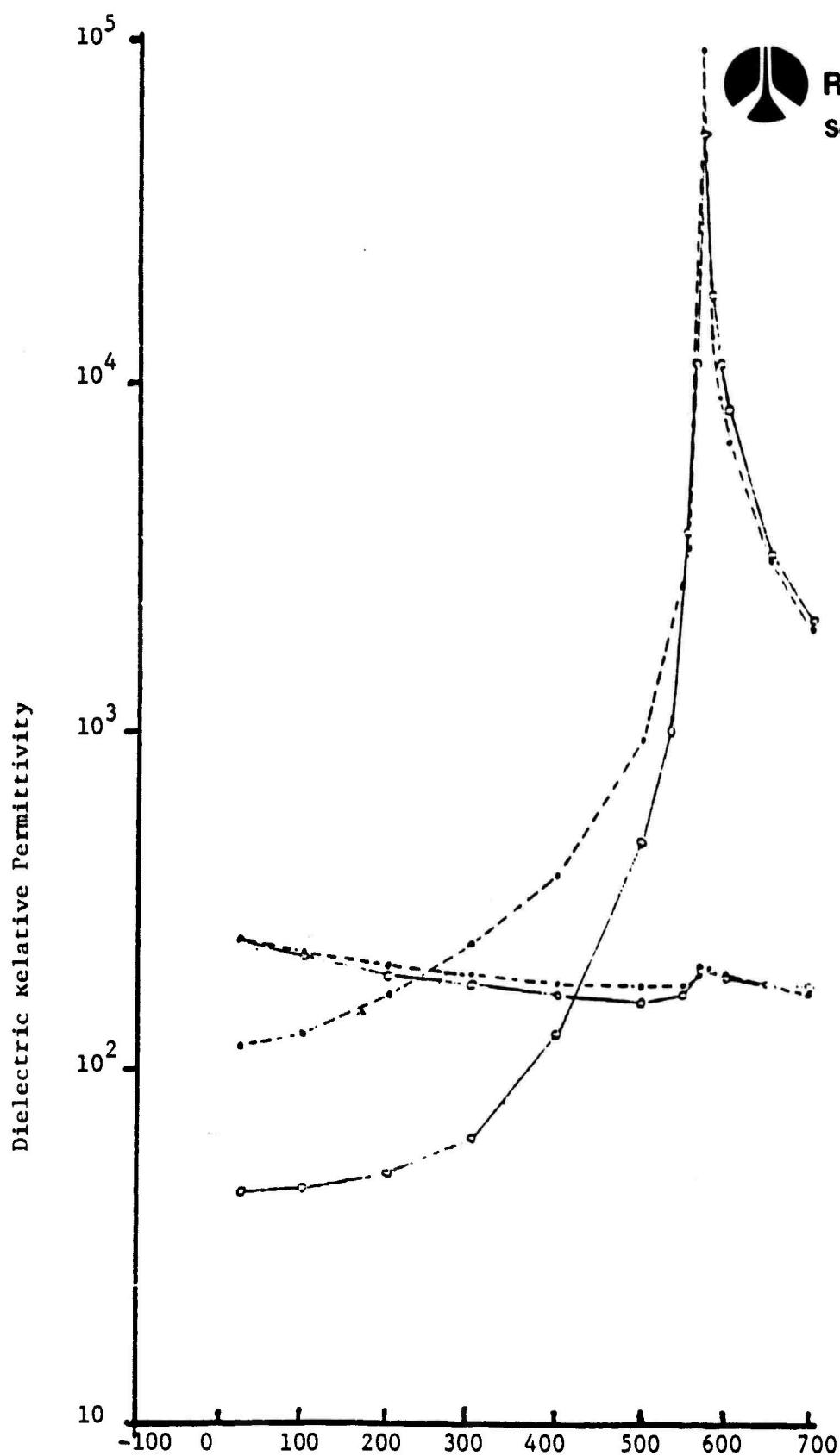|			
o	o	o	Phenomenology
Δ	Δ	Δ	Nonlinear Optical Results
+	+	+	Pyroelectric Measurement
			Optical Impermeability

T_c = 563°C.
θ_3 = 560°C.
P_{so} = 0.145 c/m².

Figure 2.   Phenomenological fitting to the dielectric permittivity in single crystal $Ba_2NaNb_5O_{15}$.

. . .   Theory.
o o o   Experiment.

Table V. Thermodynamic Constants for Tetragonal Tungsten Bronze Ferroelectric Crystals.

Compound	$1/2\ \alpha_{30}$	$12\ \alpha_{33}$	$30\ \alpha_{333}$	$1/2\ \alpha_{10}$	α_{15}
$Ba_{0.75}Sr_{0.25}Nb_2O_6$	$2.4\ 10^{-6}$	$-2.3\ 10^{-3}$	$3.6\ 1^{-1}$		
$Ba_{0.5}Sr_{0.5}Nb_2O_6$	$2.4\ 10^{-6}$	$-6.2\ 10^{-3}$	$3.2\ 10^{-1}$		
$Ba_{0.4}Sr_{0.6}Nb_2O_6$	$1.6\ 10^{-6}$	$-11.0\ 10^{-3}$	$3.6\ 10^{-1}$		
$Ba_{0.33}Sr_{0.67}Nb_2O_6$	$2.7\ 10^{-6}$	$-1.6\ 10^{-3}$	$3.1\ 10^{-1}$		
$Ba_{0.39}Sr_{0.61}Nb_2O_6$	$2.52\ 10^{-6}$	$-8.4\ 10^{-3}$	$3.6\ 10^{-1}$	$3.73\ 10^{-6}$	$2.1\ 10^{-3}$
$KSr_2Nb_5O_{15}$	$3.45\ 10^{-6}$	$-9.7\ 10^{-3}$	$3.4\ 10^{-1}$	$2.4\ 10^{-6}$	$11.3\ 10^{-3}$
$3\%\ (La)\ KSr_2Nb_5O_{15}$	$2.2\ 10^{-6}$	$-9.6\ 10^{-3}$	$2.85\ 10^{-1}$		
$6\%\ (La)\ KSr_2Nb_5O_{15}$	$2.0\ 10^{-6}$	$-10.5\ 10^{-3}$	$3.8\ 10^{-1}$		
$9\%\ (La)\ KSr_2Nb_5O_{15}$	$3.14\ 10^{-6}$	$-12.2\ 10^{-3}$	$3.58\ 10^{-1}$		
$NaB_2Nb_5O_{15}$	$3.44\ 10^{-6}$	$-11.46\ 10^{-3}$	$2.5\ 10^{-1}$	$5.15\ 10^{-6}$	$13.3\ 10^{-3}$
$Na_{1.65}Ba_{4.35}Nb_{9.65}Ti_{0.35}O_{30}$	$3.56\ 10^{-6}$	$-5.34\ 10^{-3}$	$1.63\ 10^{-1}$		
$K_3Li_2Nb_5O_{15}$	$2.87\ 10^{-6}$	$-14.16\ 10^{-3}$	$1.13\ 10^{-1}$	$2.82\ 10^{-6}$	

4.0 REFERENCES

1. L.E. Cross, R. Betsch, H. McKinstry, T. Shrout and R.R. Neurgaonkar. Proc. 34th Frequency Control Symp. (1980).

2. T.R. Shrout, L.E. Cross, P. Moses, H.A. McKinstry and R.R. Neurgaonkar. Proc. 1980 Ultrasonics Symp., 414 (1980).

3. T.R. Shrout, "A Phenomenological Theory for Predicting the Temperature Dependence of Elastic Compliance in Simple Proper Ferroelectric Tungsten Bronzes," Ph.D. Thesis in Ceramic Science, The Pennsylvania State University, May, 1981.

4. T.R. Shrout, D.A. Hukin and L.E. Cross, Ferroelectric Letters 44, 325 (1983).